Evidence for magnetic dimerons in the anisotropic bilayer system $La_{1.2}Sr_{1.8}Mn_2O_7$: An EXAFS study

T. A. O'Brien,[1] F. Bridges,[1] L. Downward,[1] J. F. Mitchell,[2] and H. Zheng[2]
[1]*Physics Department, University of California, Santa Cruz, California 95064, USA*
[2]*Argonne National Laboratory, Argonne, Illinois 60439, USA*
(Received 2 November 2005; revised manuscript received 27 October 2006; published 16 February 2007)

A temperature-dependent EXAFS investigation of $La_{1.2}Sr_{1.8}Mn_2O_7$, with x rays polarized parallel to the *c* axis and in the *ab* plane, has shown an extremely sharp and anisotropic jump in the broadening σ of the Mn-O pair-distribution function (PDF) near the ferromagnetic transition temperature, T_c. This jump is associated with an increase in Jahn-Teller (JT) distortions as the temperature increases through T_c. The data show that changes in σ^2 as T is lowered below T_c is linearly correlated with the sample magnetization, and that there is a break in the slope of this correlation when the sample is ~80% magnetized, consistent with the recently proposed dimeron model. A JT distortion clearly exists well above T_c and some distortions still remain for a range of temperatures below T_c. In agreement with recent work on the $La_{1-x}Ca_xMnO_3$ (LCMO) system, the data indicate that two types of distorted sites must occur; one is associated with the hole charge carriers (two-site polaron called a dimeron) and has a very small distortion/site; the second is associated with unpaired electron sites and has a similar distortion/site as observed for corresponding sites in LCMO. Furthermore, the broadening of the Mn-O PDF shows a second and more subtle increase above T_c near $T^* \approx 250$ K, a change in structure that correlates well with features in several other experiments.

DOI: 10.1103/PhysRevB.75.064417 PACS number(s): 75.47.Lx, 71.38.−k, 61.10.Ht, 71.27.+a

I. INTRODUCTION

In 1996, Moritomo *et al.*[1] reported a new colossal magnetoresistance (CMR) material: $La_{2-2x}Sr_{1+2x}Mn_2O_7$ (LSMO) with $x=0.4$. It is an $n=2$ Ruddlesden-Popper phase, layered perovskite, and a cousin to the archetypal CMR materials, $La_xA_{1-x}MnO_3$, where *A* is Sr, Ca, Pb, etc. Measurements on these layered manganites show a very large and anisotropic negative magnetoresistance (MR), particularly near the ferromagnetic transition temperature, T_c.

Early studies of the material by Mitchell, Argyriou, and co-workers show changes in lattice distortions, bond lengths, and Debye-Waller factors that are correlated with the ferromagnetic transition at T_c.[2–4] In addition, they report anisotropic magnetostriction within the material: contraction along the *c* axis and expansion within the *ab* plane near T_c. These studies also show some short-range magnetic order between T_c and $T^* \approx 300$ K.[3] A more recent neutron-scattering study of this material by Argyriou *et al.* shows a polaron-liquid to polaron-glass transition as the temperature is lowered through $T^* \approx 310$ K.[5] Other research on the material suggests a second transition near T^* [or even a third and fourth transition above T^* (Ref. 6)] in ac susceptibility, high-frequency magneto-impedance, and in variations of the Mn-O bond length in this temperature range.[2–4,7]

In this paper, we apply the EXAFS technique to LSMO $x=0.4$ to examine temperature-dependent changes in the local structure. We aim to show that local structure dynamics are crucial to understand CMR in this class of materials.

Although no structural studies by EXAFS have yet been published, one neutron pair distribution function (PDF) study has been carried out for the bilayer $x=0.3$ system;[8] however, this system is expected to have a different behavior from the $x=0.4$ sample considered here.[9] Some preliminary (unpublished) EXAFS results have conflicting results about the magnitude of the distortion along the *c* axis and within the *ab* plane.[10,11]

A number of EXAFS studies of the pseudocubic manganites $La_{1-x}Ca_xMnO_3$ (LCMO) have been performed (see Refs. 12–16 and references therein) to probe distortions around the Mn site as a function of temperature, sample magnetization, and hole concentration (the nominal hole concentration is approximately the dopant concentration). A summary of these results, including a recent study,[17] are the following: (i) there is a rapid increase in the broadening, σ, of the Mn-O pair distribution function [attributed to the formation of Jahn-Teller (JT) polarons] as the temperature is increased up to T_c over the entire concentration range that exhibits CMR behavior; above T_c, the increase of σ with T is slow; (ii) upon cooling below T_c, the distortion removed, $D=\Delta(\sigma^2)$, initially is small and increases linearly with the sample's magnetization M; (iii) when the fractional magnetization, $\frac{M}{M_0}$ (M_0 is the saturation magnetization at low T) reaches approximately twice the hole concentration, $2x$, there is a rapid increase in the slope of D versus $\frac{M}{M_0}$; (iv) measurements as a function of magnetic field[16,17] show that broadening associated with the formation of JT polarons is spread over a wider T range, yet the plot of D versus $\frac{M}{M_0}$ is nearly universal; the distortion D is determined primarily by M and is independent of whether the value of M is achieved via a change in B or in T.

In the most recent EXAFS work, Downward *et al.*[17] proposed a model where M develops via the aggregation of two-site polarons (Downward *et al.* call them "dimerons") or multiples of such pairs; we will use the term dimeron to refer to a two-site polaron here. The dimerons consist of pairs of coupled Mn sites with aligned spins; initially one Mn site would correspond to an e_g electron site while the other is a hole site.[17] The two Mn spins are coupled via double exchange (DE), mediated by an electron (or hole) hopping rap-

idly back and forth between the two Mn sites. In addition, because the two sites share a JT distortion between them, the net distortion per site for the pair is reduced since the electron (or hole) is partially delocalized. In this model, as the sample magnetization increases, the DE-coupled dimerons magnetize first until they have all aggregated in the magnetic clusters at $\frac{M}{M_0} \approx 2x$;[18] for further increases in M at lower T or higher B, the remaining JT-distorted Mn sites become magnetized and a larger JT distortion per site is removed. The low initial slope in a plot of D versus $\frac{M}{M_0}$ is experimental evidence that the dimeron pairs have much less distortion per site than a simple pair of Mn sites with a localized electron on one and a hole on the other. Consequently within this model, the total distortion observed near T_c should be decomposed into two contributions: (i) a fraction $2x$ of the sites (the dimeron pair sites) should have a low distortion; (ii) the remaining fraction $(1-2x)$ of unpaired Mn sites, which have an e_g electron, have a larger distortion per site, similar to (but likely smaller than) the JT distortion observed in $LaMnO_3$.

In this contribution, we present a detailed polarized EXAFS study of one of the bilayer CMR manganites. Our results show similar behavior to the pseudocubic manganites LCMO, and we find that the change in the local distortions about the Mn atoms near T_c is significantly larger in the *ab* plane compared to the *c* axis. In addition, we have also addressed the question raised in several scattering experiments that report a disappearance of polaronlike distortions below T_c and a slow disappearance of polaron correlations and distortions as T is increased above T_c.[19,20] We address both situations in the discussion.

The paper is organized as follows: a brief discussion of the sample, sample preparation and the EXAFS technique is provided in Sec. II, the data are presented in Sec. III, and the analysis is discussed in Sec. IV. Further discussion of the results relative to other measurements and a conclusion are given in Sec. V.

II. EXPERIMENTAL DETAILS AND THE EXAFS TECHNIQUE

The $La_{1.2}Sr_{1.8}Mn_2O_7$ single crystal was melt-grown in an O_2 environment using an optical image furnace as described in detail in Ref. 2. A sample slice was cut from the resulting boule with the surface roughly 45° to the *c* axis and 45° to the *ab* plane.

Mn *K*-edge EXAFS data were collected over a range of temperatures (3–300 K) at the Stanford Synchrotron Radiation Laboratory (SSRL) on beamline 10-2 and at the Advanced Photon Source (APS) on beamline BM20, using x rays with the polarization **P** in the *ab* plane or parallel to the *c* axis; this provides independent probes of the distortions in these two directions. In Fig. 1, we show the 45° sample slice and its orientation in the x-ray beam for these two polarizations.

Fits of the EXAFS data were carried out using the EXAFS equation, which is given by

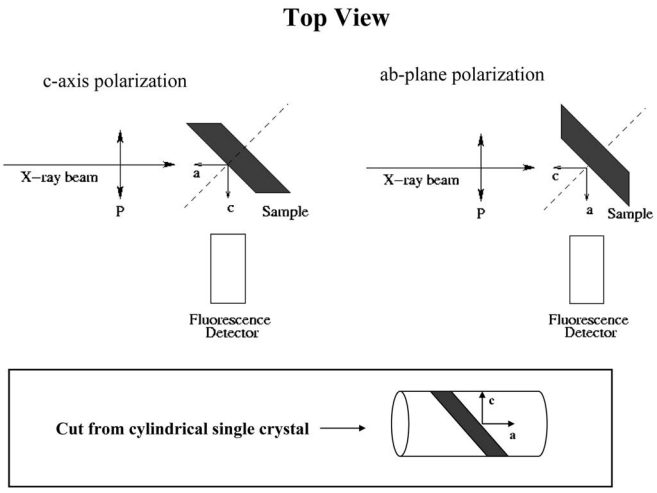

FIG. 1. A top view sketch of the experimental arrangement for collecting polarized EXAFS data for the bilayer sample. The 45° sample slice and its relationship to the crystal boule is shown at the bottom. The incident x-ray beam approaches from the left and is polarized horizontally. By placing the sample at two different orientations, the polarization **P** will be either along the *c* axis or in the *ab* plane. Since the sample is tetragonal, it does not matter whether **P** is along **a**, along **b**, or at some other orientation within the *ab* plane for this measurement.

$$k\chi(k) = \sum_i k\chi_i(k)$$

$$= \mathrm{Im}\sum_i A_i \int_0^\infty F_i(k,r)\frac{g_i(r_{0i},r)e^{i[2kr+2\delta_c(k)+\delta_i(k)]}}{r^2}dr, \quad (1)$$

$$A_i = N_i S_0^2, \quad (2)$$

where $g_i(r_{0i},r)$ is the pair distribution function (PDF) for the atoms at a distance r_{0i} (for the ith shell), $F_i(k,r)$ is the backscattering amplitude, and $\delta_c(k)$ and $\delta_i(k)$ are the phase shifts from the central and backscattering atom potentials. We will assume a Gaussian PDF with a width σ_1 for the first shell. There is also an implicit parameter, ΔE_0, that describes a difference in E_0 between the value defined for the data and the theoretical functions (for which $k=0$ at E_0). The amplitude A_i is the product of the coordination number N_i from diffraction,[2] and S_0^2, the amplitude reduction factor due mainly to multielectron excitations. The fits to be discussed shortly also require theoretical EXAFS functions—these were calculated using the code FEFF 8.10—developed by Rehr and co-workers.[21]

For comparisons of σ^2 with the sample magnetization M, we require a measure of the magnetization as a function of T at $B \sim 0$; this was obtained from the magnitude of a magnetic Bragg diffraction peak as a function of T, obtained from Osborn *et al.*[22] for this sample.

It should be noted that different contributions to σ^2 add up in quadrature if the different distortions are uncorrelated: $\sigma^2_{\mathrm{total}} = \sigma^2_{\mathrm{phonons}} + \sigma^2_{\mathrm{polarons}} + \sigma^2_{\mathrm{static}}$. Within the model proposed by Downward *et al.*,[17] the "polaron" contribution for the *x*

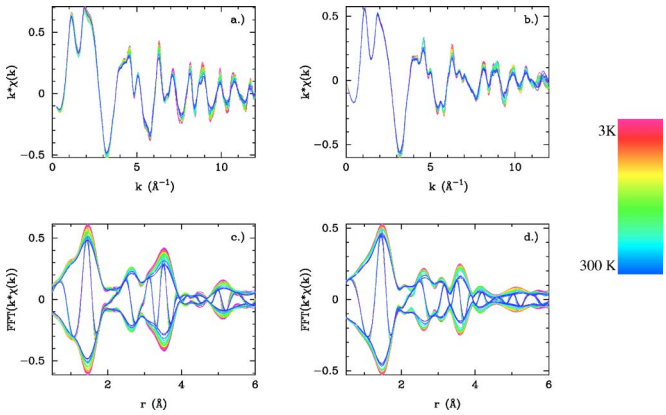

FIG. 2. (Color online) EXAFS data for one experimental run for LSMO, $x=0.4$, *ab*-plane and *c*-axis polarizations, from 3 to 300 K. (a) $k\chi(k)$ vs k, *ab* plane; (b) $k\chi(k)$ vs k, *c* axis; (c) FFT$[k\chi(k)]$ vs r, *ab* plane; (d) FFT$[k\chi(k)]$ vs r, *c* axis. For all four figures, the lowest temperature has the highest amplitude, which decreases with increasing temperature. For the FT data, the fast oscillation is the real part of the transform FT_R, while the envelope is $\pm\sqrt{\mathrm{FT}_R^2+\mathrm{FT}_I^2}$. [$k$-space FT window, 3.0–11.0 Å^{-1}, Gaussian broadened by 0.3 Å^{-1}.]

$=0.4$ sample should be further subdivided into two contributions: 80% of the sites covered by the dimerons (two site polarons), $\sigma^2_{\mathrm{dimerons}}$, and the remaining 20% of JT distorted electron sites, σ^2_{JT}.

III. DATA

The data were reduced using the RSXAP package,[23] which implements standard EXAFS reduction techniques. A pre-edge background was removed and an experimental E_0 was defined as the energy of the half-height point on the edge. The post-edge background was removed using a spline with five or six knots to approximate μ_0 in $\mu(E)=\mu_0[1+\chi(E)]$, and a self-absorption correction for the fluorescence data was applied.[24] The background-subtracted data were transformed to k space using the relation $k=\sqrt{\frac{2m(E-E_0)}{\hbar^2}}$; examples of the k-space data for $T=3$ K are shown in Figs. 2(a) and 2(b).

Next the k-space data were fast Fourier transformed (FFT) to r space with a k-space window of $k=[3.0-11.0$ Å$^{-1}]$ with Gaussian tails of width 0.3 Å^{-1}. Examples of the resulting r-space data are shown in Figs. 2(c) and 2(d).

IV. ANALYSIS

The data were fit to FEFF8.10-generated theoretical EXAFS functions[21] using the program `rsfit` (RSXAP package[23]). Our primary interest here is the Mn-O PDF, which has four O neighbors (O3) in the *ab* plane and two different O neighbors (O1, O2) along the *c* axis. See Fig. 3 for reference. For each polarization, the number of oxygen neighbors was fixed at the value(s) determined from the structure. In such fits, a number of other constraints on the parameters are also required. First, ΔE_0 was obtained by allowing σ and ΔE_0 to vary on the lowest-temperature data within a set (a set being data collected at the same facility, on the same beam-line, in

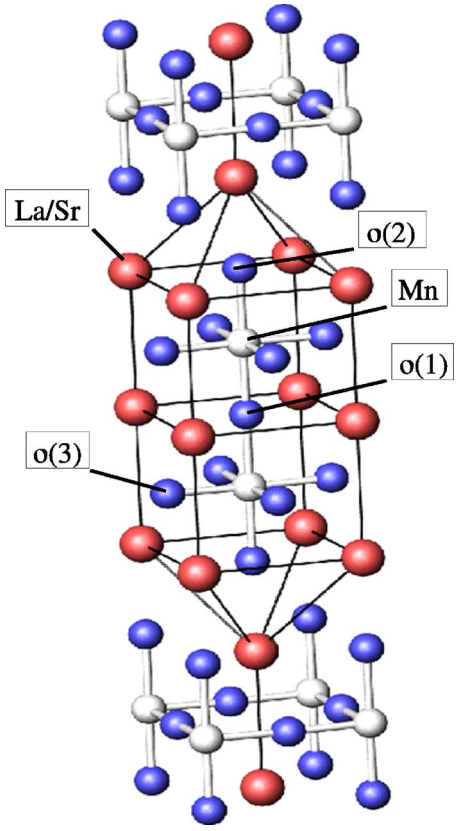

FIG. 3. (Color online) A computer rendition of approximately one unit cell of $La_{2-2x}Sr_{1+2x}Mn_2O_7$. Note that O3 lies in the *ab* plane and is fourfold-degenerate relative to Mn, and that the non-degenerate O1 and O2 lie along the *c* axis. The red spheres represent the La/Sr site, the white spheres represent the Mn site, and the blue spheres represent the O sites.

the same run) and then using the value obtained from that fit to constrain ΔE_0 for the rest of the data in that set. Second, because we want a single measure of the local distortions, we used only one value of σ for the Mn-O shell (for each x-ray polarization). For the parameter S_0^2, a number of fits were carried out. S_0^2 is an amplitude correction factor that is included to correct for multielectron effects, since multielectron absorption contributes to the edge step height but not to the EXAFS amplitude. However, it also corrects for several other small effects: small errors in the estimation of the mean free path in the theoretical calculations and a small amplitude reduction in the data because of the x-ray energy resolution and/or some harmonic content in the synchrotron beam (or pinholes in powder samples). The main effect of small changes in this parameter is a nearly rigid vertical shift of plots of σ^2 verus T; to lowest order, the temperature dependence is unchanged and an effective static component is added (or subtracted). In the first set of fits, we let the amplitude A_1 vary ($A_1=N_1S_0^2$) for the low-temperature *ab*-plane data and determined S_0^2 from those fits. Then A_1 was kept constant for fits as a function of T. Further discussion about setting S_0^2 is given later.

The constraints on Δr (the change in bond length) differ for the two polarization orientations because there is one average Mn-O3 distance in the *ab* plane but two distinct

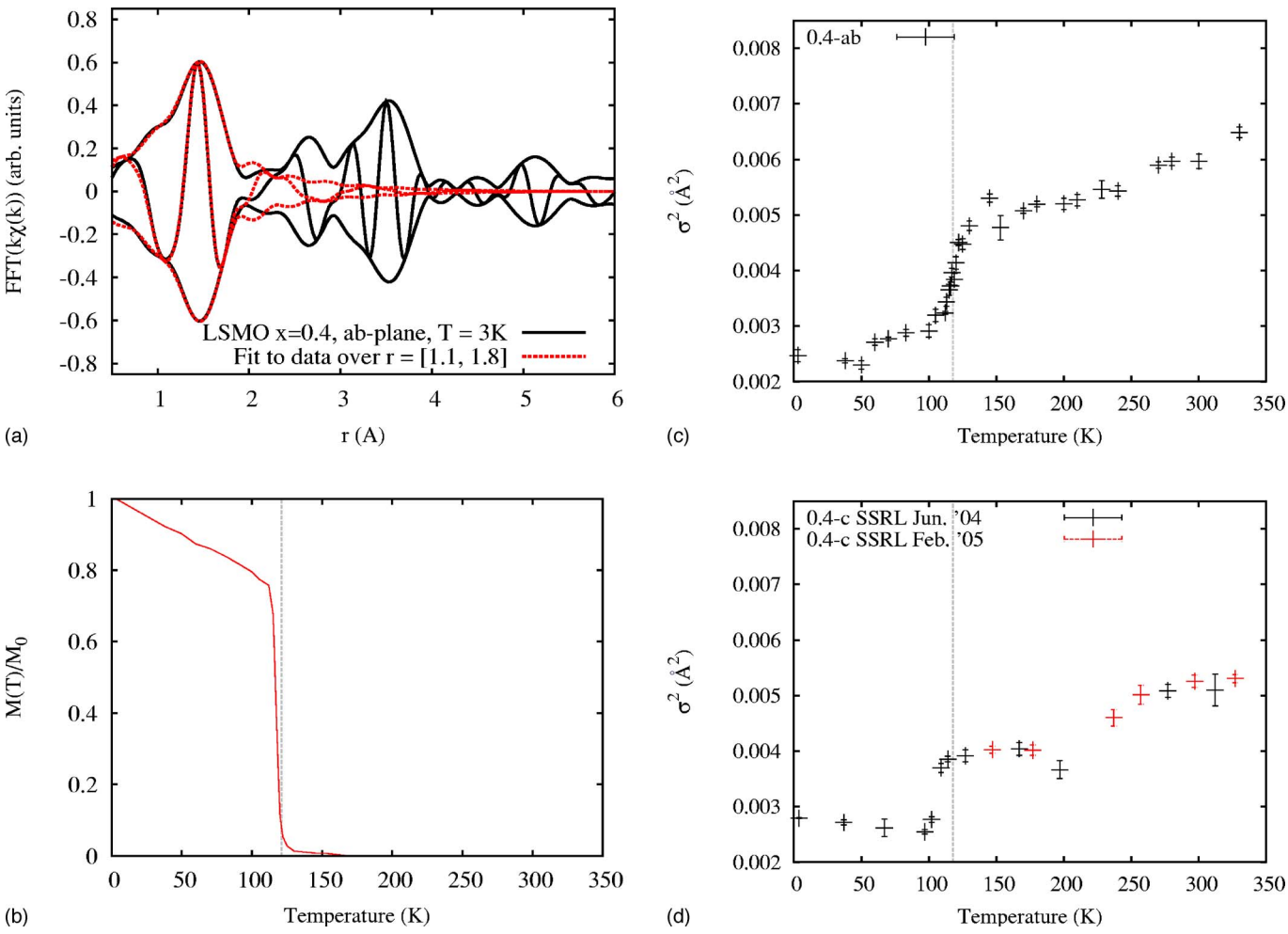

FIG. 4. (Color online) (a) Fit of Mn-O3 peak from $r=1.1$ to 1.8. (b) Fractional magnetization vs T for LSMO $x=0.4$. (c) σ^2 vs T for LSMO, $x=0.4$, $\mathbf{P}$ in the ab plane. (d) σ^2 vs T for LSMO, $x=0.4$, $\mathbf{P}\|\mathbf{c}$.

distances along the c axis. Initially the Δr's were allowed to vary; for both the ab-plane and the c-axis data, we found that $r_{\mathrm{EXAFS}}(T) \approx r_{\mathrm{diffraction}}(T)$ within our error bars. However, for the c-axis data there is a correlation between r and σ because of the two distinct bond lengths along the c axis (Mn-O1 and Mn-O2); a small variation in the splitting between these two bond lengths shows up as a variation in the average value of σ for the c-axis data. To minimize such fluctuations for the $\mathbf{P}\|\mathbf{c}$ polarization, the Δr's for Mn-O1 and Mn-O2 were constrained to the values from the diffraction data.[2] In contrast, for the ab-plane data there is very little variation in σ with r and correlations between r and σ were not an issue. Figure 4(a) shows examples of such a fit in r space.

Figure 4 shows $\sigma^2(T)$ for both the ab plane and the c axis.[25] The change in σ^2 is extremely sharp at T_c and approximately follows the magnetization data[26] [Fig. 4(b)] for both polarizations; we attribute this jump to a large increase in the Jahn-Teller distortions about the Mn site, associated with dimerons and some isolated JT distorted sites, as the temperature is increased through T_c. The magnitude of this jump in σ^2 is about 65% larger for the ab-plane data than for the c-axis results, which indicates that more long bonds develop in the ab plane than along the c axis. In addition, Fig. 4 also suggests a second smaller jump in σ^2 just below 300 K, which will be discussed later.

It should be noted that for the February 2005 data set in Fig. 4(d) we had to use a shorter FT range, 4.5–10.0 Å^{-1}, as there were two to three sample diffraction glitches that could not be reliably removed above this range, and good fits could not be obtained for $k_{\mathrm{min}} < 4.5$ Å^{-1}.

Following our earlier analysis for the pseudocubic LCMO system,[17] the next step is to determine the thermal phonon contributions so that the contribution from JT distortions can be extracted as a function of T. First we provide the equations used to describe the T dependence of σ^2 from phonons. In the simplest case for which the Einstein approximation is appropriate (typically when an optical mode or local mode vibration dominates),

$$\sigma^2_{\mathrm{Einstein}} = \frac{\hbar^2}{2M_R k_B \Theta_E} \coth \frac{\Theta_E}{2T}, \tag{3}$$

where M_R is a reduced mass (the Mn-O reduced mass here), Θ_E is the Einstein temperature, and k_B is Boltzmann's constant; at low T one obtains the zero-point motion while at high T, $\sigma^2 = k_B T/\kappa$, where κ is the effective spring constant.

For all phonon modes[27] including acoustic phonons, the correlated Debye model is usually a better approximation,[28–30]

$$\sigma^2_{c\mathrm{Debye}} = \frac{3\hbar}{2M_R}\int_0^{\omega_D} \frac{\omega}{\omega_D^3} C_{ij} \coth\left(\frac{\hbar\omega}{2k_BT}\right) d\omega; \qquad (4)$$

here ω_D is the Debye frequency, C_{ij} is a correlation function given by $1-\sin(\omega r_{ij}/c)/(\omega r_{ij}/c)$, and $c=\frac{\omega_D}{k_D}$, where k_D is the Debye wavelength. Again $\sigma^2(T=0)$ gives the zero-point motion value of σ^2. The slope of $\sigma^2(T)$ versus T is very low at low T and increases to a constant value (determined by the spring constant, reduced mass, and C_{ij}) for $T>\Theta_D$. Sometimes the Debye model is restricted to only the acoustic phonons; in that case, if there are several atoms per unit cell, then σ^2 will be a sum of terms of the form given in Eqs. (3) and (4).

For both polarizations, we first tried fitting the σ^2 verus T data above T_c (125–350 K) to a correlated Debye model plus a static offset (i.e., ignoring for now the small jump between 250 and 300 K). For the *ab*-plane data, this led to $\Theta_D=716$ K and a large static offset (expected to be mainly from the JT distortions/dimerons). However, if the static offset is then set to zero, the zero-point motion contribution to $\sigma^2_{\mathrm{Debye}}$ at low T ($\leq$20 K) is much higher than the experimental value of σ^2($\sim$3 K); to match this Debye curve to the data at low T would require $S_0^2\approx 0.87$—this value is much higher than is observed for all our Mn *K*-edge data and suggests that Θ_D is higher than 716 K. If instead one fits the low T values of σ^2 for the *ab*-plane data to the zero-point motion value within a correlated Debye model, then Θ_D $\sim$850–900 K. Furthermore, since the Mn-O bond lengths in the bilayer material do not change appreciably from those in the pseudocubic material, the stiffness should be comparable; therefore, we set $\Theta_D=860$ K—a value that describes this bond strength in both the Ca- and Sr-substituted $LaMnO_3$ materials[12,17,31] and is also consistent with our low-T value for σ^2. This also provides a systematic means of correcting the data collected on different beamlines and with different monochromator crystals, so that they can be combined. For each data set, S_0^2 was set such that the low-temperature $\sigma^2(T)$ data are consistent with the zero-point motion value given by a Debye model with $\Theta_D=860$ K; this method yielded values of S_0^2 between 0.78 and 0.81 for each data set. Such tiny variations in S_0^2 manifest as small static, vertical shifts in $\sigma^2(T)$.

For $\Theta_D=860$ K, the Debye model plus a static offset, passes through the points just above T_c (125–200 K) very well (see Fig. 5), much better than for the fit with Θ_D =716 K, but the resulting curve is clearly below the high-T data ($T>250$ K) as shown in Fig. 5(b). A second fit with $\Theta_D=860$ K and a larger static offset passes through the high-T data well and makes the step clearer. This second transition, which occurs between 250 and 290 K, correlates quite well with features observed in other measurements.[2–4,6,7] Similarly, for the *c*-axis data, a fit over the restricted range 125–175 K yields $\Theta_D\sim 860$ K.

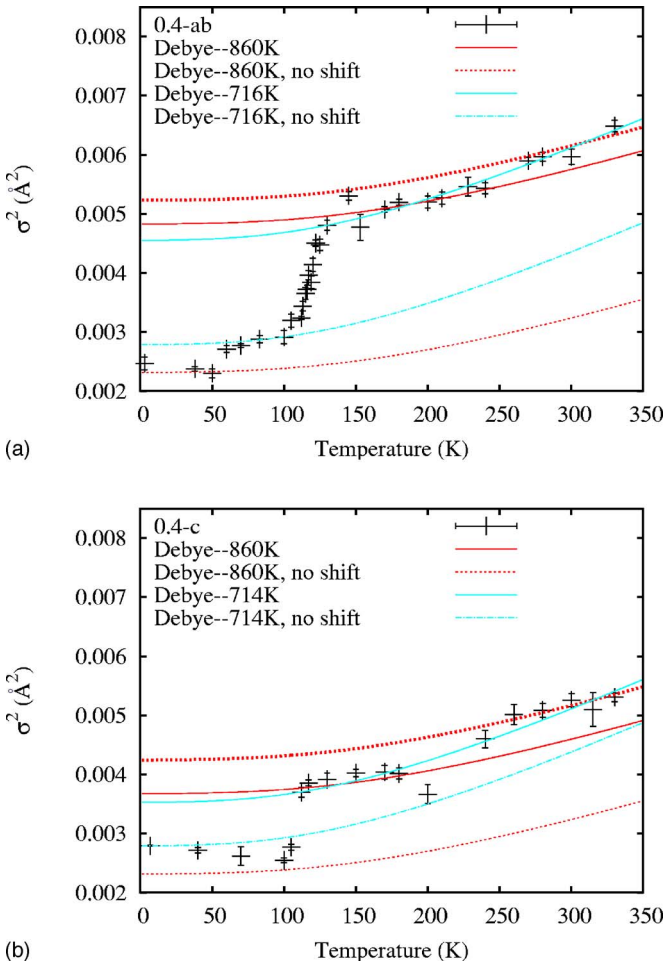

FIG. 5. (Color online) (a) σ^2 vs T for LSMO, $x=0.4$, **P** in the *ab* plane. (b) σ^2 vs T for LSMO, $x=0.4$, **P**$\|$**c**.

The nonphonon, JT/dimeron distortion, σ^2_{JT}, is now obtained by subtracting the correlated Debye model from the *ab*-plane σ^2 data as shown in Fig. 6. This background includes very small static distortions at low T. Just above T_c, the plot is horizontal. For decreasing temperatures, we define the distortion removed as the sample becomes magnetized $[D=\Delta(\sigma^2)]$ as the difference between the horizontal line and $\sigma^2_{\mathrm{JT}}(T)$ as shown in Fig. 6.

Values of $\Delta(\sigma^2)$ as a function of $\frac{M}{M_0}$ (from Osborn *et al.*[22]) were obtained for LSMO $x=0.4$ in the same manner as for the quasicubic system (LCMO)[17] and are plotted in Fig. 7. As in the quasicubic system, a break in slope appears when most of the sample has been magnetized and $\frac{M}{M_0}\sim 2x$ ($\frac{M}{M_0}\sim 0.8$ for $x=0.4$); the slope for $\frac{M}{M_0}<0.8$ is significantly smaller than for $\frac{M}{M_0}>0.8$. This provides evidence that a dimeronlike quasiparticle also exists in the bilayer manganites and that, as for LCMO, one needs to consider two types of distorted sites in this system: one associated with the hole charge carriers (dimeron or two-site polaron) and another with the remaining JT-distorted Mn sites.

The ratio of the slopes above and below the breakpoint is comparable to that observed in the pseudocubic LCMO system for which the ratio of the two slopes is $\sim$4.[16,17] The individual slopes, m, for the $x=0.4$ bilayer sample are given

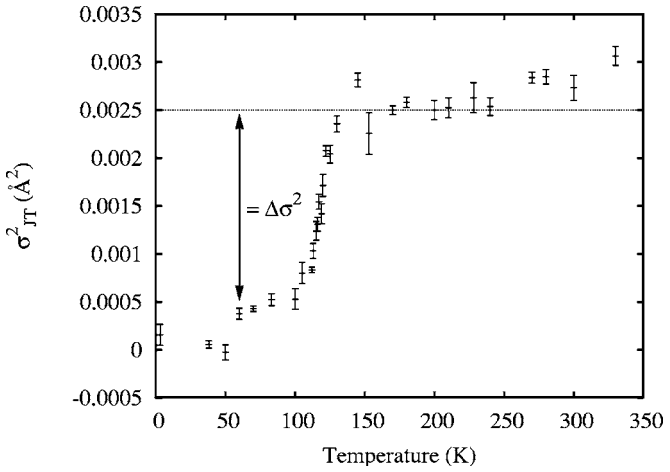

FIG. 6. The nonphonon contribution to the broadening, σ^2_{JT}, obtained by subtracting the correlated Debye fit ((Fig. 4) from the data. Note that it is level just above T_c as indicated by the horizontal line. The decrease in JT distortion, $\Delta(\sigma^2)$, as T decreases below T_c is defined as the difference between the horizontal line and $\sigma^2_{JT}(T)$.

in the legend (Fig. 7); their ratio is ~3.2. A comparison with the absolute slopes for the LCMO system shows that the high slopes for the two systems are quite similar—the high slope for the bilayer LSMO (x=0.4) is the same as that for the 40% Ca LCMO sample within the error of the slopes.

Whether the quasiparticles that form the ferromagnetic domains are isolated dimerons or clusters of dimerons cannot be determined from our data; it only requires that such quasiparticles contain equal numbers of hole and electron sites. Additional evidence for clustering comes from inverse susceptibility $[\chi^{-1}(T)]$ data of Gu *et al.*,[32] which show a deviation from the Curie-Weiss law. For $120<T<280$ K, the slope of $\chi^{-1}(T)$ suggests clusters of four to five Mn moments. Similar data from Velázquez *et al.*[6] also show a deviation from the Curie-Weiss law, but over a much larger temperature range. Their data suggest three approximately linear regimes, which give ~4 Mn-site clusters in the T_c to 270 K range, ~2 Mn-site clusters for $300<T<480$ K, and single

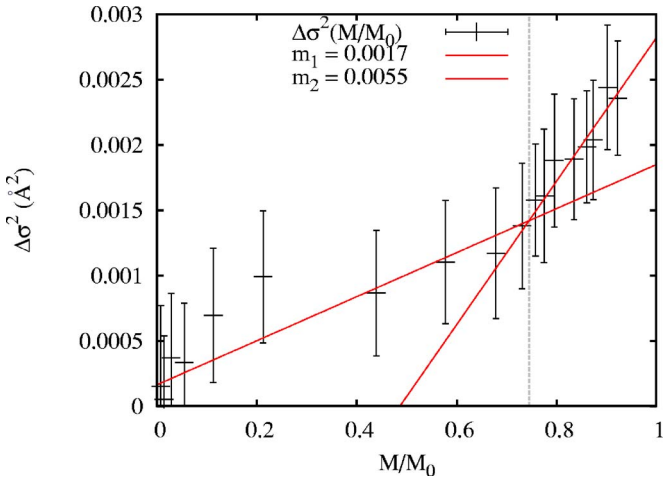

FIG. 7. (Color online) $\Delta(\sigma^2)$ vs $\frac{M}{M_0}$ for LSMO x=0.4 *ab* plane. We estimate the error on the slopes to be around 20%.

Mn sites (localized electron and hole sites) in the high-T range ($480<T<600$ K).

For the *c*-axis data, the interpretation is more complicated because of the two distinct Mn-O bonds (Mn-O1 and Mn-O2). Since small changes in the splitting of these bond lengths can mimic a change in σ^2 (and two bond lengths are required in the fits), there is a larger systematic uncertainty for this polarization orientation. The magnitude of the step at T_c is clearly smaller than for the *ab* plane, and the *c*-axis data above T_c are again suggestive of a second small step with a transition within the range 200–260 K, possibly slightly lower than for the *ab* plane. However, the data are not good enough to determine either the step size or the step position as accurately as for the *ab*-plane data. In addition, the *c*-axis data suggest, at a 1-sigma statistical level, that there is a slight increase in σ^2 at low T; it is as yet unclear whether or not this is a real effect or the result of using bond lengths fixed at the values from diffraction.

V. DISCUSSION AND CONCLUSIONS

It is important to note that if the magnetization develops uniformly throughout the sample, i.e., the domains are compact and all the Mn sites are considered equivalent in terms of magnetization, then when a fraction y of the sample has been magnetized, a fraction y of the electron (Jahn-Teller active) sites within this domain should be magnetized as well. Within this model, we have the following dependencies on the fraction of magnetized sites at a hole concentration x:

$$\Delta(\sigma^2)(y) \propto y(1-x), \tag{5}$$

$$M(y) = y[x\mu_1 + \mu_2(1-x)], \tag{6}$$

where μ_1 and μ_2 are the moments of the hole and electron sites, respectively. Since both $M(y)$ and $\Delta(\sigma^2)(y)$ are a linear function of y, $\Delta(\sigma^2)$ would be a linear function of $\frac{M}{M_0}$ over the entire range and not have a strong break in slope. This argument does not change if there are fluctuating sites as long as all Mn sites are equivalent magnetic sites. The two distinct slopes in Fig. 7 show directly that there are two types of sites.

The JT distortions for this sample are shown in Fig. 6; note that some JT/dimeron distortion persists *below* T_c, and that it decreases as the magnetization increases to its saturation value at very low temperatures (see Fig. 7). In contrast, in the analysis of diffuse scattering data in Refs. 19 and 20, the authors have assumed that there are no JT distortions below T_c and use a straight line through the low-T data as the background thermal phonon contribution.[19,20] In addition, the EXAFS data also evince the persistence of JT-like distortions far *above* T_c, which also contrasts with the background-subtracted diffuse scattering results; Vasiliu-Doloc *et al.* report a large decrease (~80%) in the scattering from individual polarons (from the Huang scattering) at 300 K.[19,20] However, a review of the total diffuse scattering (which includes the small diffuse phonon scattering contribution in addition to Huang scattering) and the EXAFS σ^2 data without any background subtraction indicates that these two very

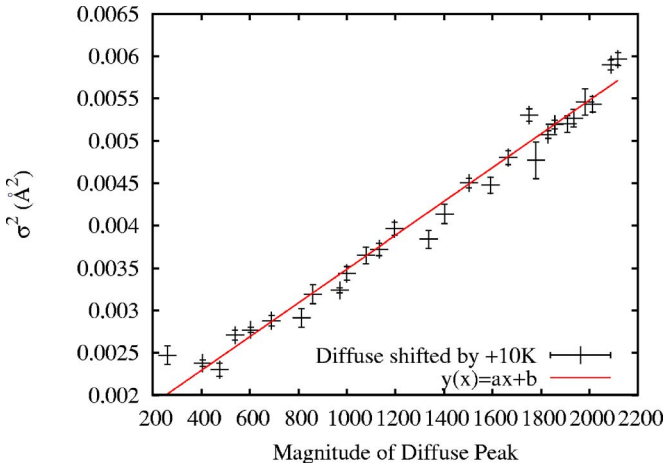

FIG. 8. (Color online) The correlation between the width of the Mn-O pair distribution function and the diffuse scattering amplitude. The scale of the correlation (the slope) is 2.0 $\times 10^{-6}$ Å^2/count.

different data sets look surprisingly similar. To explore this we plotted σ^2 versus total diffuse scattering; the only correction used was to account for the slightly different temperature at which the step occurs—the step in the diffuse scattering occurs slightly below that in the magnetization plot while the step in the EXAFS is slightly above the magnetization step. With this slight correction, the plot—which covers the entire temperature range from 10 to 300 K—is very linear, as shown in Fig. 8. This demonstrates a very striking relationship between the diffuse scattering and σ^2 for the Mn-O bond, which needs to be explored further; however, that is beyond the scope of this paper. Additional work will be needed to understand these similarities and differences.

In conclusion, results of an EXAFS study of the bilayer perovskite, $La_{1.2}Sr_{1.8}Mn_2O_7$, show that polaronlike distortions (a two-site polaron, which we refer to as a dimeron) exist for $T > T_c$ as in the quasicubic manganites. As the magnetization increases near and below T_c, JT/dimeron distortions disappear from the system: the distortion and the magnetization are linearly correlated, but the dimeron distortion initially removed is small. There is a break in the linear slope of distortion versus magnetization when most of the sample has been magnetized; the break in the slope occurs roughly when $\frac{M}{M_0}$ is twice the hole concentration, $2x$. This provides further evidence that there are two types of distortions in the CMR manganites. The sample initially becomes magnetized via the aggregation of dimeron pairs or clusters of pairs, which have a reduced Jahn-Teller distortion and contain the hole carriers. The small remaining fraction of electron sites must have a large distortion per site and become magnetized when $\frac{M}{M_0} > 0.8$, presumably via a proximity effect.

Furthermore, the data show evidence for a second step in distortion, for $T^* \approx 250$ K, in the c axis and a similar transition in the ab plane. This T^* is near but slightly below a T^* reported by Argyriou and others, below which the material shows short-range order down to T_c.[3] It is also where the amplitude of an incoherent peak becomes small, which has been interpreted as a decrease in the size of the polaron clusters.[19,20] This may suggest that these small polaron clusters (dimeron clusters) have slightly less average distortion per Mn site than the single dimerons.

ACKNOWLEDGMENTS

We would like to thank R. Osborn *et al.* for providing a copy of their magnetization data for our use. Also we would like to thank Géza Kurczveil for help in preparing various figures. The work at UCSC was supported by NSF Grant No. DMR0301971. The experiments were performed at SSRL (operated by the DOE, Division of Chemical Sciences, and by the NIH, Biomedical Resource Technology Program, Division of Research Resources) and at the PNC-CAT at the APS. The PNC-CAT facilities are supported by the U.S. DOE Office of Science Grant No. DEFG03-97ER45628, the University of Washington, a major facilities access grant from NSERC, Simon Fraser University, and the APS. Use of the APS is also supported by the U.S. DOE Offices of Science and Basic Science, Contract No. W-31-109-Eng-38.

[1] Y. Moritomo, A. Asamitsu, H. Kuwahara, and Y. Tokura, Nature (London) **380**, 141 (1996).
[2] J. F. Mitchell, D. N. Argyriou, J. D. Jorgensen, D. G. Hinks, C. D. Potter, and S. D. Bader, Phys. Rev. B **55**, 63 (1997).
[3] D. N. Argyriou, J. F. Mitchell, C. D. Potter, S. D. Bader, R. Kleb, and J. D. Jorgensen, Phys. Rev. B **55**, R11965 (1997).
[4] D. N. Argyriou, H. N. Bordallo, J. F. Mitchell, J. D. Jorgensen, and G. F. Strouse, Phys. Rev. B **60**, 6200 (1999).
[5] D. N. Argyriou, J. W. Lynn, R. Osborn, B. Campbell, J. F. Mitchell, U. Ruett, H. N. Bordallo, A. Wildes, and C. D. Ling, Phys. Rev. Lett. **89**, 036401 (2002).
[6] M. Velázquez, A. Revolevschi, J. P. Renard, and C. Dupas, Eur. Phys. J. B **23**, 307 (2001).
[7] P. V. Patanjali, P. Theule, Z. Zhai, N. Hakim, S. Sridhar, R. Suryanarayanan, M. Apostu, G. Dhalenne, and A. Revcolevschi, Phys. Rev. B **60**, 9268 (1999).
[8] D. Louca, G. H. Kwei, and J. F. Mitchell, Phys. Rev. Lett. **80**, 3811 (1998).
[9] M. Medarde, J. F. Mitchell, J. E. Millburn, S. Short, and J. D. Jorgensen, Phys. Rev. Lett. **83**, 1223 (1999).
[10] P. Villella, S. Conradson, J. Espinosa, Y. Tokura, and D. Dessau, Bull. Am. Phys. Soc. **43**, 293 (1998).
[11] J. Linton, S. Bader, D. Li, D. Haskell, M. Newville, G. Knapp, and J. Mitchell, Bull. Am. Phys. Soc. **44**, 1913 (1999).
[12] C. H. Booth, F. Bridges, G. H. Kwei, J. M. Lawrence, A. L. Cornelius, and J. J. Neumeier, Phys. Rev. B **57**, 10440 (1998).
[13] G. Subías, J. García, M. G. Proietti, and J. Blasco, Phys. Rev. B **56**, 8183 (1997).
[14] A. Lanzara, N. L. Saini, M. Brunelli, F. Natali, A. Bianconi, P. G. Radaelli, and S.-W. Cheong, Phys. Rev. Lett. **81**, 878 (1998).

[15] D. Cao, F. Bridges, C. H. Booth, and J. J. Neumeier, Phys. Rev. B **62**, 8954 (2000).
[16] L. M. Downward, F. Bridges, D. Cao, J. Neumeier, and L. Zhou, Int. J. Mod. Phys. B **17**, 3726 (2003).
[17] L. Downward, F. Bridges, S. Bushart, J. Neumeier, N. Dilley, and L. Zhou, Phys. Rev. Lett. **95**, 106401 (2005).
[18] Downward *et al.* argue that these dimeron pairs probably form at some temperature T^* above T_c.[17]
[19] L. Vasiliu-Doloc, S. Rosenkranz, R. Osborn, S. K. Sinha, J. W. Lynn, J. Mesot, O. H. Seeck, G. Preosti, A. J. Fedro, and J. F. Mitchell, Phys. Rev. Lett. **83**, 4393 (1999).
[20] L. Vasiliu-Doloc, R. Osborn, S. Rosenkranz, J. Mesot, J. F. Mitchell, S. K. Sinha, O. H. Seeck, J. W. Lynn, and Z. Islam, J. Appl. Phys. **89**, 6840 (2001).
[21] A. L. Ankudinov, B. Ravel, J. J. Rehr, and S. D. Conradson, Phys. Rev. B **58**, 7565 (1998).
[22] R. Osborn, S. Rosenkranz, D. N. Argyriou, L. Vasiliu-Doloc, J. W. Lynn, S. K. Sinha, J. F. Mitchell, K. E. Gray, and S. D. Bader, Phys. Rev. Lett. **81**, 3964 (1998).
[23] C. H. Booth, R-Space X-ray Absorption Package, http://lise.lbl.gov/RSXAP/.
[24] C. H. Booth and F. Bridges, Phys. Scr. **T115**, 202 (2005).
[25] Though there are two slightly different Mn-O bond lengths along the *c* axis, each with their own distribution function, the same σ is used to describe the broadening. The main reason is to have a single parameter describing the overall distortion to compare the results for the two polarization orientations and with $\frac{M}{M_0}$. In addition, `rsfit` could not successfully resolve one peak from the other if σ and r were allowed to vary for both peaks.
[26] The magnetization from neutron diffraction (magnetic Bragg peak) is very sharp at low M, while both the EXAFS and the bulk magnetization show rounding. We have combined the two magnetization measurements as follows: Because of magnetic domain effects in the bulk measurements at high M, we have used only the magnetization from neutron diffraction above $\frac{M}{M_0} \approx 0.7$. Below 0.7, we have averaged the two results. Without our inclusion of rounding, all the points below $\frac{M}{M_0} \approx 0.3$ would shift below 0.
[27] N. W. Ashcroft and N. D. Mermin, in *Solid State Physics* (Saunders College, Philadelphia, 1976).
[28] G. Beni and P. M. Platzman, Phys. Rev. B **14**, 1514 (1976).
[29] B. K. Teo, *EXAFS: Basic Principles and Data Analysis* (Springer-Verlag, New York, 1986).
[30] *X-Ray Absorption Principles Applications Techniques of EXAFS SEXAFS XANES*, edited by D. Koningsberger and R. Prins (Wiley, New York, 1988).
[31] N. Mannella, A. Rosenhahn, C. H. Booth, S. Marchesini, B. S. Mun, S.-H. Yang, K. Ibrahim, Y. Tomioka, and C. S. Fadley, Phys. Rev. Lett. **92**, 166401 (2004).
[32] J. Y. Gu, S. D. Bader, H. Zheng, J. F. Mitchell, and J. E. Gordon, Phys. Rev. B **70**, 054418 (2004).